





**Bathtub vortex effect on Torricelli's law**A. Caquas <sup>1,2</sup>, L. R. Pastur <sup>1,\*</sup>, A. Genty <sup>2</sup> and P. Gondret <sup>3</sup><sup>1</sup>*Unité de Mécanique, ENSTA Paris, Institut Polytechnique de Paris, Palaiseau, France*<sup>2</sup>*Université Paris-Saclay, CEA, Service de Thermo-hydraulique et de Mécanique des Fluides, Gif-sur-Yvette F-91191, France*<sup>3</sup>*Université Paris-Saclay, CNRS, Laboratoire FAST, Orsay F-91405, France*

(Received 27 July 2022; accepted 28 March 2023; published 25 April 2023)

We investigate experimentally the unsteady draining flow from a rotating tank. The fluid in the tank is first set in solid rotation, before the draining hole is opened. We show that the draining may be drastically reduced by the rotation, as the vortex circulation increases together with the surface deformation. We demonstrate that the usual Torricelli's draining law has to be modified with the surface deformation and that the draining time is mainly governed by a nondimensional parameter corresponding to the ratio of the size of the outlet to the thickness of the Ekman boundary layer.

DOI: [10.1103/PhysRevFluids.8.044702](https://doi.org/10.1103/PhysRevFluids.8.044702)**I. INTRODUCTION**

Nearly four centuries ago, Torricelli discovered the law describing the emptying of a vessel under the acceleration due to gravity  $g$  [1]. This law, which was demonstrated one century later by Bernoulli when neglecting viscous dissipation [2], relates the draining velocity  $v_T$  to the mean water level  $H$  above the bottom hole,  $v_T(t) = \sqrt{2gH(t)}$ , at any time  $t$ , for a hole of section  $s$  much smaller than the section  $S$  of the vessel. The evolution of  $H(t)$  established from mass conservation leads to the total draining time  $T_0 = (S/s)\sqrt{2H_0/g}$ . Many works devoted to the emptying of tanks with a free surface in the open air focus on some discrepancies between this theoretical law and experimental data [3–9]. These discrepancies can be taken into account by using a corrective coefficient  $\beta < 1$  in the draining law, i.e.,  $v_{\beta T} = \beta v_T$ . Many subtle phenomena come into play near the outlet. From a simple analysis of the *vena contracta* of the water jet,  $\beta$  can be as small as  $1/2$  [10] but other phenomena such as wetting effects give rise to experimental  $\beta$  values from 0.64 to 0.93, depending on the geometry of the outlet but also on its size relative to the capillary length [9]. The total draining time  $T_\beta$  is thus expected to be  $1/\beta$  longer than its ideal value  $T_0$ .

In contrast to small vessels such as bottles of water where a vortex can hardly be observed without rotation, a vortex appears during the draining of large open-air tanks. This is a common observation for emptying baths, but this also occurs at much larger scales in environmental or industrial situations, for instance in the case of hydraulic dams with a loss of efficiency and wear of equipment [11–13] or in the case of nuclear power plants with major safety issues [14–16]. The emptying process is an incredible amplifier of vorticity and the popular experiments of Shapiro [17] and Trefethen *et al.* [18] perfectly illustrate this phenomenon. Carried out under very controlled conditions, they are like the Foucault's pendulum, part of the human-scale demonstrations of the Earth's rotation [19,20].

When the fluid is drained without any rotation, the flow structure is simple with a point sink flow close to the outlet section and connected far away to a downward uniform flow. The structure of

\*Corresponding author: [luc.pastur@ensta-paris.fr](mailto:luc.pastur@ensta-paris.fr)

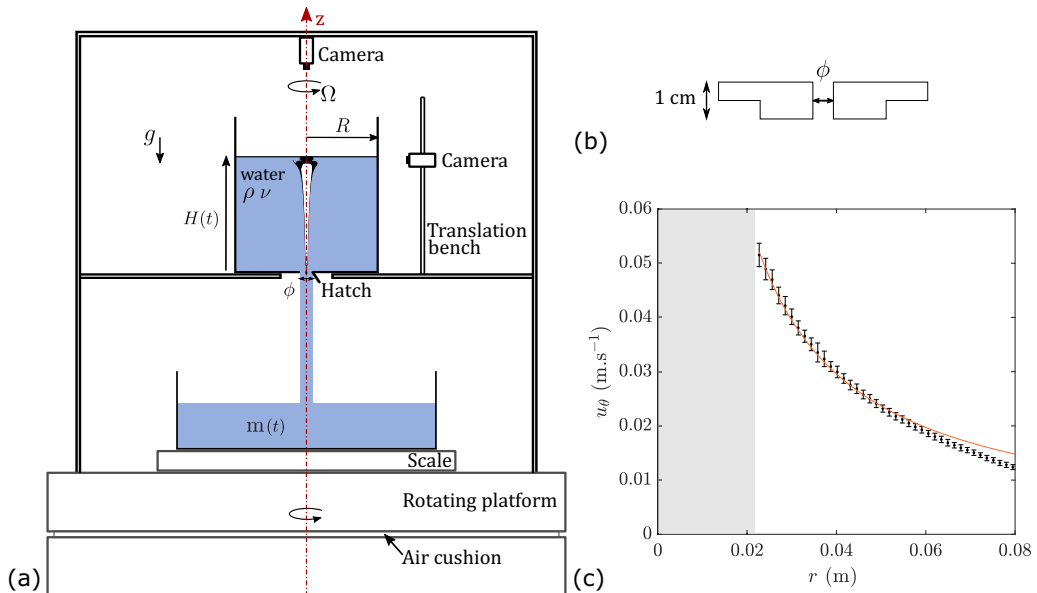


FIG. 1. Schematic drawing of (a) the experimental setup and (b) the outlet cylindrical draining pieces. (c) Typical radial dependence of the azimuthal velocity  $u_\theta(r)$ : experimental data from PIV measurements for  $\Omega = 5$  rpm,  $\phi_1$ , and at  $t = 2000$  s (black symbols), and Rankine's model fit of equation  $u_\theta = \Gamma/2\pi r$  with  $\Gamma = 7.4 \times 10^{-3} \text{ m}^2 \text{ s}^{-1}$  (orange solid line). The gray area corresponds to a zone where the distorted interface prevents correct azimuthal velocity measurements.

the vortex flow is more complex. It consists of several regions that have been studied under steady conditions, i.e., at constant water level  $H$  [21–36]. Two distinct regions of the flow contribute to the emptying. The boundary layer at the interface is drained within a fine pipe region above the outlet. A part of the Ekman boundary layer that develops at the bottom wall of the tank flows directly into the outlet section while the remaining part is pumped upwards and forms complex structures in the bulk. Andersen *et al.* [27,29] estimated that the flow rate  $Q_E$  coming from the Ekman boundary layer accounts for 90% of the total drained flow  $Q$  and found the relation  $Q_E = \Gamma\delta/2$  where  $\delta$  is the thickness of the boundary layer and  $\Gamma$  is the velocity circulation associated with the vortex. It is worth noting that the vortex flow characterized by its circulation and core size deforms the free surface accordingly [36].

Although differences in draining velocities with and without a vortex have been reported in steady conditions [29], to our knowledge, no study has been done to investigate in detail the influence of vortex flow on the unsteady Torricelli's law. In this article, we address this question with a rotating vessel. We show that a transition between two different draining regimes takes place resulting in a slower draining in the case of rotation. The study of bathtub vortex in a rotating reference frame is widely used [27,29,33–35] and allows the vortex to be controlled in intensity and stabilized on the axis of rotation, avoiding possible complex precession motion.

## II. EXPERIMENTAL SETUP

Our rotating platform consists of two 20-cm-thick cylindrical marble pieces of diameter 1.5 m, piled up together and separated by a 1-mm-thick air cushion, which allows the upper piece to rotate without solid friction around the vertical axis of rotation  $Oz$  [a sketch of the experimental setup is shown in Fig. 1(a)]. The rotation velocity  $\Omega$  can be changed from 0 to 10 rpm. A Plexiglas cylinder

of radius  $R = 145 \pm 0.1$  mm and length 390 mm whose bottom plate is drilled in its center is mounted on a metal frame in the rotating platform and is centered along  $Oz$ . The leveling is ensured with a precision of  $\pm 0.1^\circ$ . Three different cylindrical draining pieces are made of PVC (1 cm thick) with internal holes of diameter  $\phi_1 = 2.9 \pm 0.1$  mm,  $\phi_2 = 3.5 \pm 0.1$  mm, or  $\phi_3 = 4.0 \pm 0.1$  mm, respectively [see Fig. 1(b)]. The top of the draining pieces is flush with the bottom wall of the tank. An hermetic hatch leans against the bottom and can be remotely removed at  $t = 0$  s, at which the initial level of water is  $H_0 = 375 \pm 1$  mm. The rotation is imposed during the entire experiment and 1 h before the draining starts at  $t = 0$  s, to be sure that the bulk is initially in solid body rotation. The typical spin-up time  $H_0/(\nu\Omega)^{1/2}$  [37,38] which holds for cylindrical geometry and in the presence of a free surface [34,39] is actually of the order of  $10^3$  s, smaller than the settling time of 1 h. The initial parabolic deformation of the interface  $\Omega^2 R^2/4g$  is less than 0.3 mm, thus negligible. We use chlorinated water with a surface tension  $\sigma$  of  $58 \pm 4$  mN m $^{-1}$ , density  $\rho$  of  $998$  kg m $^{-3}$ , and kinematic viscosity  $\nu$  of  $(1.03 \pm 0.02) \times 10^{-6}$  m $^2$  s $^{-1}$  at the regulated room temperature  $19 \pm 1$  °C. The Ekman number  $\text{Ek} = \nu/\Omega R^2$  is thus in the range  $6.7 \times 10^{-5} \leq \text{Ek} \leq 2.3 \times 10^{-4}$ .

The cumulative mass  $m(t)$  of drained water at time  $t$  is measured with a precision of 0.5 g and a sampling frequency of 7 Hz. The scale is centered on  $Oz$ , such that no inertial correction is required for the weight measurement. The mean level of water in the tank is deduced as  $H(t) = H_0 - m(t)/\rho\pi R^2$  within an accuracy of 1 mm. The flow rate  $Q = \dot{m}/\rho$  is determined from the time derivative of  $m$  by using a Savitzky-Golay polynomial interpolation of  $m(t)$  at time  $t$  over eight successive points of measurement [40]. Two video cameras are placed in the rotating frame to track the free surface and the velocity in the bulk. From the side of the tank, every 10 s we capture the axisymmetric radial profile of the water level  $h(r, t)$ , which satisfies  $\frac{1}{\pi R^2} \int_0^R h(r, t) 2\pi r dr = H(t) \simeq h(R, t)$ . The radial and azimuthal components ( $u_r, u_\theta$ ) of the velocity field in the rotating frame are measured in a horizontal plane located 1.5 cm above the bottom of the tank using a thin horizontal 670-nm laser sheet and a camera from above thanks to a particle image velocimetry (PIV) technique. The frame rate of the camera is adjusted between 20 and 60 Hz for the correlation of two successive images and the mean velocity field is obtained from ten successive velocity fields. Immediately after the PIV measurement, the ambient light is automatically switched on to make the  $h(r, t)$  measurement. When the water surface is deformed by the vortex core, the particle displacements in the PIV plane cannot be correctly determined close to  $Oz$ . Thus, the core radius,  $r_c$ , of the vortex cannot be directly determined in our experiment. However, we can determine the vortex circulation,  $\Gamma$ , from the expected variation in azimuthal velocity,  $\Gamma/(2\pi r)$ . The Rankine model should be valid in the irrotational region outside the Stewartson boundary layer of thickness  $R \times \text{Ek}^{1/4} \approx 2$  cm, thus far enough from the sidewall [29,35]. In our experiments, the validity region is shorter due to the unsteady nature of the draining. Figure 1(c) shows a typical experimental curve of  $u_\theta(r)$ , as well as the corresponding fitting curve that provides the value of  $\Gamma$ .

### III. EFFECT OF ROTATION ON DRAINING

Figure 2(a) shows some typical time evolutions of the draining velocity  $v_Q(t) = Q(t)/\pi(\phi/2)^2$  for different rotation velocity  $\Omega$  and hole diameter  $\phi$ , where  $v_Q$  and  $t$  are made dimensionless with the initial velocity value  $\sqrt{2gH_0}$  and total draining time  $T_0 = (2R/\phi)^2 \sqrt{2H_0/g}$  for an ideal Torricelli's law, respectively. In such a dimensionless plot, an ideal Torricelli draining would follow a straight line of slope  $-1$  starting from  $(0,1)$ . Without rotation, the draining curves are straight lines with a correction coefficient  $\beta = 0.90 \pm 0.03$  close to 1 as the hole diameter  $\phi$  is of the order of the capillary length  $\ell_c = (\gamma/\rho g)^{1/2} \simeq 3$  mm [9].

When the rotation is large enough, the draining curves are no longer straight lines but a drastic reduction of the draining velocity appears during the discharge. This reduction leads to a significant increase of the experimental draining time  $T$  for increasing  $\Omega$  as shown in Fig. 2(b) for all  $\Omega$  and  $\phi$ . The time  $T(\Omega)$ , defined as the time for which 99% of the initial water level has been drained, increases with  $\Omega$  by a factor that increases with increasing  $\phi$ , up to twice  $T(0)$  for the largest  $\Omega$  and

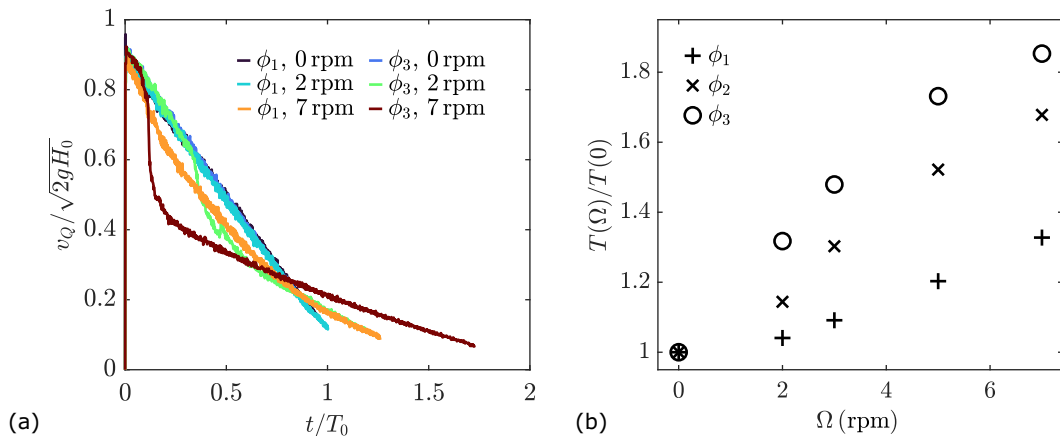


FIG. 2. (a) Time evolution of  $v_Q/\sqrt{2gH_0}$  for  $\phi = \phi_1$  and  $\phi_3$ , and  $\Omega = [0, 2, 7]$  rpm. The time  $t$  is scaled by  $T_0 = (2R/\phi)^2\sqrt{2H_0/g}$ . (b) Experimental draining time  $T(\Omega)$  scaled by  $T(0)$  as a function of  $\Omega$  for  $\phi_1$ ,  $\phi_2$ , and  $\phi_3$ .

$\phi$ . This phenomenon is observed to be closely related to the deformation of the free surface during the discharge.

#### IV. DRAINING MODEL FROM SURFACE DEFORMATION

Typical photographs of the interface evolution are displayed in Figs. 3(a)–3(c) for  $\Omega = 2$  rpm and  $\phi_2$ . Initially, the interface remains flat and the draining curve does not deviate from Torricelli’s law, with  $v_Q = v_{\beta T}$ , even when the vortex is well formed in the bulk. The free surface then slightly deepens above the hole [ $\approx 3$  mm in Fig. 3(a)] as the vorticity concentrates, which is accompanied by a slight decrease of the draining velocity [ $\approx 1\%$  in Fig. 3(e)]. The air core continues to deepen [ $\approx 2$  cm in Fig. 3(b)], with now a significant drop in the draining velocity [ $\approx 4\%$  in Fig. 3(e)].

The reduction of the draining velocity  $v_Q$  compared to the usual value  $v_{\beta T}$  can be understood by considering the momentum balance equations in the rotating frame. When neglecting surface tension effects [36], the pressure distribution  $p$  in the bulk can be considered as hydrostatic:

$$p(r, z) = p_0 + \rho g[h(r) - z], \quad (1)$$

where  $p_0$  is the atmospheric pressure at the free surface.

Following Milne-Thomson [10] and Andersen *et al.* [29], the viscous terms in the momentum equation can be neglected. Under the quasistatic approximation, the momentum equation integrated over the whole fluid domain  $\mathcal{D}$  of surface  $S_c$  [see Fig. 3(d)] reduces to

$$\mathbf{e}_z \cdot \iint_{S_c} \rho \mathbf{u}(\mathbf{u} \cdot \mathbf{dS}) = -2\pi \rho g \int_0^R h(r) r dr - \mathbf{e}_z \cdot \iint_{S_c} p \mathbf{dS} \quad (2)$$

along the  $z$  axis, the projection of the centrifugal and Coriolis forces being zero following this axis. By considering the uniform draining velocity  $v_{\text{eff}}$  a little below the outlet where the jet section is  $s_{\text{eff}} = \pi(\phi_{\text{eff}}/2)^2$  and where the pressure is  $p_0$ , Eq. (2) yields

$$\rho v_{\text{eff}}^2 s_{\text{eff}} = 2\pi \rho g \int_0^{\phi/2} h(r) r dr. \quad (3)$$

In the simple case without surface deformation, when  $h(r, t) = H(t)$ , the *vena contracta* should correspond to  $s_{\text{eff}}/s = (\phi_{\text{eff}}/\phi)^2 = 1/2$  as recalled in the introduction from Bernoulli’s theorem [10]. In the more general case with surface deformation, the draining velocity takes

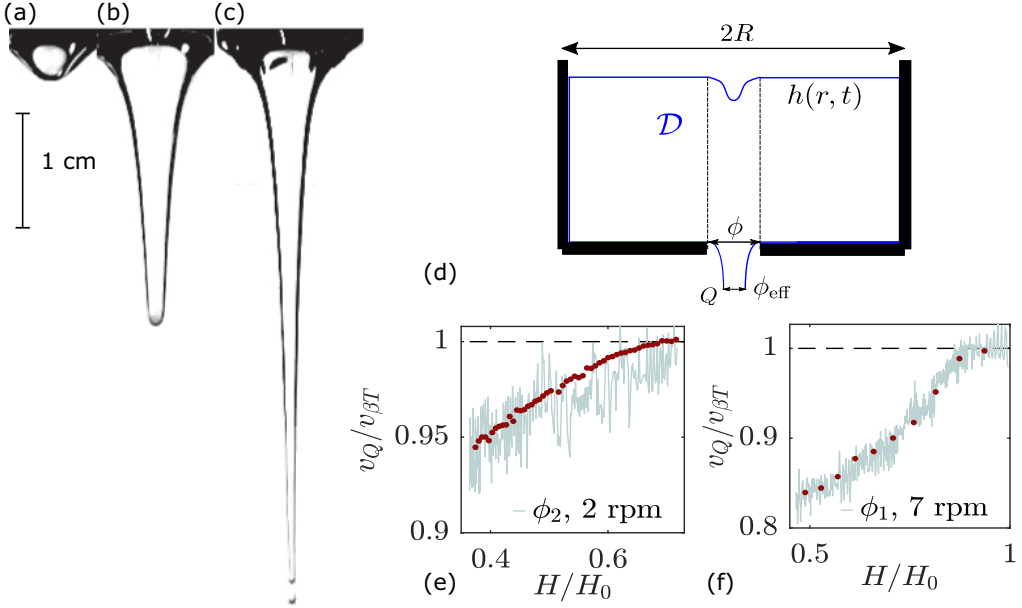


FIG. 3. (a)–(c) Photographs of the interface during the emptying for  $\Omega = 2$  rpm and  $\phi_2$  at (a)  $H(t = 396 \text{ s})/H_0 = 0.66$ , (b)  $H(t = 696 \text{ s})/H_0 = 0.46$ , and (c)  $H(t = 1006 \text{ s})/H_0 = 0.3$ . At that moment, bubbles are formed and carried down the outlet from the tip of the vortex. (d) Schematic drawing of the tank and fluid domain  $\mathcal{D}$  (in blue), which includes the volume of water in the tank and the contracted jet at the outlet. (e), (f) Draining velocity  $v_Q$  scaled by  $v_{\beta T}$  as a function of the instantaneous water height  $H$  scaled by its initial value  $H_0$  for (e)  $\phi_2$  and  $\Omega = 2$  rpm, and (f)  $\phi_1$  and  $\Omega = 7$  rpm. The gray curve corresponds to mass measurements and the red points to Eq. (4) with interface shape measurements. The black dashed line shows the reference value  $v_Q = v_{\beta T}$ .

the form

$$v_Q(t) = \beta \sqrt{\frac{4g}{(\phi/2)^2} \int_0^{\phi/2} h(r, t) r dr}. \quad (4)$$

This general equation relates the draining velocity to the shape of the free surface above the hole without any modeling of the interface shape. When the free surface deepens locally due to a strong enough bathtub vortex, the draining is thus expected to be decreased accordingly. This prediction can be tested in our well-controlled rotating experiments.

Figures 3(e) and 3(f) show the agreement between the draining velocity calculated from Eq. (4) using the experimental profiles of the interface and the draining velocity measured by the mass derivative for two cases with different  $\Omega$  and  $\phi$ . While Torricelli's law systematically overestimates the draining velocity by up to 20%, the present model remains within a 3% range. When the interface starts to be destabilized with some oscillations due to bubble entrainment from the tip [Fig. 3(c)],  $h(r, t)$  can no longer be measured with confidence. This phenomenon of bubble entrainment is well known in the literature [41,42].

Let us emphasize that Eq. (4) is established for the entire emptying process, regardless of whether the Ekman boundary layer is established or not. When the boundary layer is established, the flow structure is comparable to that observed under steady-state conditions, as illustrated in the inset of Fig. 4(a). The water flux through the Ekman layer at the bottom of the container of thickness  $\delta = \sqrt{\nu/\Omega}$  is  $Q_E = \Gamma \delta/2 \simeq Q$  [27,29], giving us a useful link between the discharge flow rate  $Q$  and the circulation  $\Gamma$ . A typical time evolution of the Ekman draining velocity  $v_E(t) = Q_E(t)/\pi(\phi/2)^2$

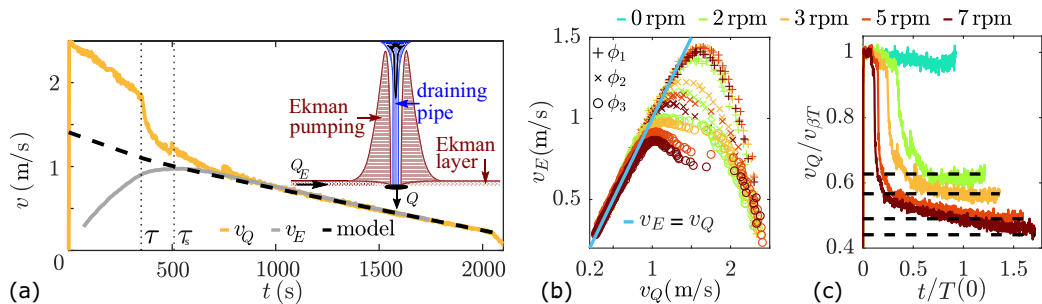


FIG. 4. (a) Time evolution of the draining velocity  $v_Q(t)$  (orange curve) and the Ekman draining velocity  $v_E(t) = \Gamma(t)\delta/[2\pi(\phi/2)^2]$  (gray curve) for  $\Omega = 3$  rpm and  $\phi_3$ . The black dashed line corresponds to Eq. (9). The two vertical dotted lines correspond to the time  $\tau$  at which the draining velocity significantly deviates from the usual Torricelli's velocity and to the time  $\tau_s$  at which the supercritical regime appears. The inset shows the flow structure in the steady case: the Ekman boundary layer and pumping (in red), and the draining pipe (in blue). (b) Evolution of the Ekman draining velocity  $v_E$  with the total draining velocity  $v_Q$  for all  $\Omega$  and  $\phi$ . The blue line corresponds to  $v_E = v_Q$ . (c) Time evolution of  $v_Q$  scaled by  $\beta\sqrt{2gH}$  for  $\phi_3$  and  $\Omega = [0, 2, 3, 5, 7]$  rpm, where the time  $t$  is scaled by  $T(0)$ . The dashed lines correspond to the values from Eq. (9) for  $\Omega \neq 0$ .

is shown in Fig. 4(a);  $v_E$  first increases, reaches a maximum ( $t \approx 500$  s), and eventually decreases. The total draining velocity  $v_Q$  decreases during the entire emptying process with an abrupt drop-off at  $\tau \approx 350$  s. Then, the gaseous core extends to the outlet section at  $\tau_s \approx 500$  s and  $v_Q$  almost merges with  $v_E$ . During this final stage of the draining process ( $t \gtrsim 700$  s), both velocities decrease linearly. This important result is common to all experiments with rotation as shown in Fig. 4(b), where  $v_E$  is plotted as a function of  $v_Q$ : at the first stage of each experiment,  $v_E$  increases when  $v_Q$  decreases, but the remarkable observation is that all the curves collapse onto the straight line  $v_E = v_Q$  in the final stage of the draining. In our experiments, this last stage occurs after a transient time ranging approximately from 11 to 23 min which accounts for one-quarter to one-half of the total emptying time.

## V. SUPERCRITICAL REGIME

In most of our experiments, at a critical stage of the draining, the gaseous core extends to the outlet section. This so-called supercritical regime [31] happens faster the greater the rotation and the larger the hole size. In this regime, the interface shape should be governed by the circulation of the vortex  $\Gamma$  [43]:

$$h(r, t) = h(R, t) - \frac{\Gamma(t)^2}{8\pi^2 gr^2}, \quad (5)$$

for  $\phi_g/2 \leq r \leq R$ , where  $\phi_g(t) = \sqrt{\Gamma(t)^2/[2\pi^2 gh(R, t)]}$  is the diameter of the gas core at the outlet. The model presented in Eq. (5) is not intended to perfectly fit the shape of the interface, which has been the subject of many studies [31,44]. Instead, it serves as an intermediary for predicting the draining velocity based on characteristic quantities of the problem ( $H$ ,  $\Omega$ ,  $\nu$ ,  $\phi$ , and  $\beta$ ). Equations (4) and (5) yield

$$v_Q(t) = \beta \sqrt{\frac{4g}{(\phi/2)^2} \int_{\phi_g/2}^{\phi/2} \left( h(R, t) - \frac{\Gamma(t)^2}{8\pi^2 gr^2} \right) r dr}, \quad (6)$$

where  $v_Q = Q/\pi(\phi/2)^2$  represents the average velocity calculated over the entire emptying section, including the gaseous core, and can therefore be directly compared to the experimentally measured

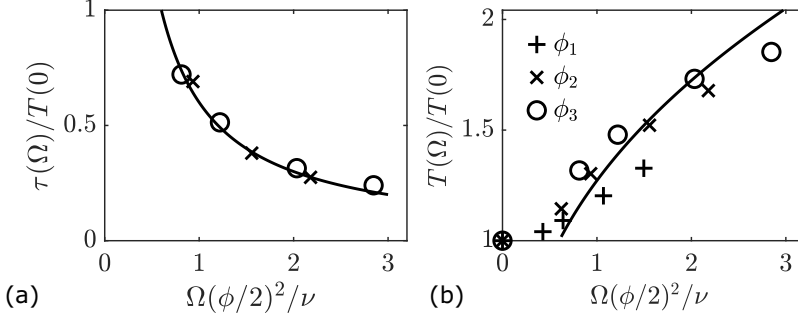


FIG. 5. (a) Transition time  $\tau$  and (b) draining time  $T$ , both normalized by  $T(0)$ , as a function of  $\Omega(\phi/2)^2/\nu$ . Same symbols as in Fig. 2(b). The solid lines correspond (a) to the best power fit  $\tau/T(0) = 0.6\nu/\Omega(\phi/2)^2$  of the data and (b) to the estimate  $T/T(0) = \tau/T(0) + [1 - \tau/T(0)](v_Q/v_{\beta T})^{-1}$ , with  $\tau/T(0)$  given by the power fit of (a) and  $v_Q/v_{\beta T}$  by Eq. (9) with  $\beta = 0.9$ .

draining velocity of the container. Integrating Eq. (6) yields

$$v_Q(t) = \beta \sqrt{2gh(R, t)} \left\{ 1 + \frac{\Gamma^2}{2gh(R, t)\pi^2\phi^2} \left[ -1 + 2 \ln \left( \frac{\Gamma}{\sqrt{2gh(R, t)}\pi\phi} \right) \right] \right\}^{1/2}. \quad (7)$$

Considering that the total flow rate  $Q \simeq \Gamma\delta/2$ , Eq. (7) reads

$$A \left( \frac{v_Q}{v_T^*} \right)^2 \left[ 1 + \frac{1}{\beta^2 A} - 2 \ln \left( A^{1/2} \frac{v_Q}{v_T^*} \right) \right] - 1 = 0, \quad (8)$$

where  $v_T^* = \sqrt{2gh(R, t)} \simeq v_T$  and  $A = (\phi/2\delta)^2$  is a dimensionless parameter corresponding to the ratio between the outlet radius  $\phi/2$  and the thickness of the boundary layer  $\delta = \sqrt{\nu/\Omega}$ . The solution of Eq. (8) reads

$$\frac{v_Q}{v_{\beta T}} = \frac{1}{\beta \sqrt{-AW_{-1}(-e^{-(1+1/\beta^2 A)})}}, \quad (9)$$

where  $W_{-1}$  is the analytic continuation of the product logarithm function. The draining velocity  $v_Q$  in the supercritical regime is thus expected to be proportional to the Torricelli's velocity  $v_{\beta T}$  with a factor depending only on the dimensionless parameter  $A = \Omega(\phi/2)^2/\nu = (\phi/2R)^2 \text{Ek}^{-1}$ . The values of  $v_Q$  predicted by Eq. (9) for  $\phi_3$  and  $\Omega = 3$  rpm is shown with a dashed line in Fig. 4(a) and matches very well with the experimental data when  $v_Q = v_E$ . The values of  $v_Q/v_{\beta T}$  from Eq. (9) compared to experimental measurements are also shown for  $\phi_3$  and different  $\Omega$  in Fig. 4(c). The agreement is very good as shown by the plateau values observed for the experimental measurements in the final discharge regime. These plateau values, ranging from 0.62 to 0.43 as  $\Omega$  increases, mean that the discharge is strongly reduced by the rotation-induced vortex. This strong reduction appears earlier as  $\Omega$  increases.

The time  $\tau$  at which the draining velocity significantly deviates from the usual Torricelli's velocity, as shown in Fig. 4(a), is displayed in Fig. 5(a) for different  $\Omega$  and  $\phi$  as a function of  $\Omega(\phi/2)^2/\nu$ . All data are clustered on a master curve whose best fit is  $\tau/T(0) = 0.6[\Omega(\phi/2)^2/\nu]^{-1}$ . This implies that the draining time should not be affected significantly by rotation [ $T(\Omega) \simeq T(0)$ ] if  $\tau/T(0) > 1$ , which corresponds to the condition  $\Omega(\phi/2)^2/\nu < 0.6$ . When  $\Omega(\phi/2)^2/\nu > 0.6$ , an estimate of the draining time can be inferred by considering the fraction of draining time in the supercritical regime, which should correspond to  $1 - \tau/T(0)$ :  $T(\Omega)/T(0) \simeq \tau/T(0) + [1 - \tau/T(0)](v_Q/v_{\beta T})^{-1}$ . This prediction, shown by a solid line in Fig. 5(b), is in good agreement with all the experimental data of Fig. 2(b), which means that  $\Omega(\phi/2)^2/\nu$  is the relevant parameter and that the present model catches the main physics.

## VI. DISCUSSION AND CONCLUSION

The present experimental study shows that the law of discharge for a water tank obeys a generalized Torricelli's law in which the mean water level must be replaced by the local level above the outlet section. The increase in the vortex strength increases the deformation of the free surface and consequently decreases the draining velocity and increases the draining time. A model that considers draining mainly through the Ekman boundary layers predicts that the increase in the emptying time for a rotating tank is mainly governed by the nondimensional parameter  $\Omega(\phi/2)^2/\nu$ , which writes also as  $(\phi/2R)^2\text{Ek}^{-1}$ , involving the Ekman number  $\text{Ek} = \nu/\Omega R^2$ . The typical time at which the unsteady draining starts to deviate from Torricelli's law scales as  $T_0(2R/\phi)^2\text{Ek} \propto (R^2/\phi^4)(\nu/\Omega)(H_0/g)^{1/2}$ , which is very different from the typical spin-up time  $H_0/(\nu\Omega)^{1/2}$ . Our model predictions are in good agreement with our experimental measurements (with deviations of less than 3%), even though we did not account for the effects of surface tension in our model. As a result, the pressure term in Eq. (1) is overestimated, and the draining velocity obtained with our model is slightly underestimated. However, we believe that the effect of surface tension in our experiments is second order. Gas entrainment [see Fig. 3(c)], which is an instability related to surface tension, is also not taken into account in our model. However, this phenomenon is only present for a duration that is not representative of our experiments. The consideration of these different effects on the draining velocity could be an interesting perspective of our work.

In order to be able to predict the draining law in the supercritical regime, we used the model Eq. (5) for the interface shape. Such a model would not be suitable in the subcritical regime, where the interface has not yet reached the outlet. In such a subcritical regime, another model could be used instead of Eq. (5) to model the interface shape, also based on the Rankine model, but this would have very limited relevance to our experiments. Indeed, in our experiments, the predominant regime when the boundary layers are established is the supercritical regime.

For larger scale experiments with a larger outlet section, we believe that the present model Eq. (4) would still be valid. For a smaller outlet section, we expect surface tension effects to be non-negligible so that the present model should be refined accordingly.

## ACKNOWLEDGMENTS

The authors acknowledge F. Moisy, W. Herreman, M. Rabaud, and A. Archer for inspiring discussions, and T. Pichon, L. Cherfa, and N. Baudet for their technical support.

- 
- [1] E. Torricelli, *Opera Geometrica [De sphaera et Solidis Spharalibus; De Motu Graviorum; De Dimensione Parabolae]* (Amadoro Massa & Lorenzo de Landis, Florence, 1644).
  - [2] D. Bernoulli, *Hydrodynamica: Sive de Viribus et Motibus Fluidorum Commentarii* (Johannis Reinholdi Dulseckeri, Strassburg, 1738).
  - [3] J. Boussinesq, Essai sur la théorie de l'écoulement d'un liquide par un orifice en mince paroi, C. R. [Comptes Rendus des Sances de l'Académie des Sciences. Paris.] **70**, 33 (1870).
  - [4] H. Judd and R. S. King, Some experiments on the frictionless orifice, Eng. News **56**, 326 (1906).
  - [5] G. F. Davidson, Experiments on the flow of viscous fluids through orifices, *Proc. R. Soc. London, Ser. A* **89**, 91 (1913).
  - [6] G. L. Tuve and R. E. Sprenkle, Orifice discharge coefficients for viscous liquids, *Instruments* **6**, 201 (1933).
  - [7] F. W. Medaugh and G. D. Johnson, Investigation of the discharge and coefficients of small circular orifices, *Civil Eng.* **10**, 422 (1940).
  - [8] C. Clanet, Clepsydrae, from Galilei to Torricelli, *Phys. Fluids* **12**, 2743 (2000).
  - [9] J. Ferrand, L. Favreau, S. Joubaud, and E. Freyssingéas, Wetting Effect on Torricelli's Law, *Phys. Rev. Lett.* **117**, 248002 (2016).



- [10] L. M. Milne-Thomson, *Theoretical Hydrodynamics* (Dover, New York, 1996).
- [11] G. Möller, M. Detert, and R. Boes, Air entrainment due to vortices: State-of-the-art, in *Proceedings of the 2nd Congress of the European Division of IAHR, Munich, Germany* (European Division of IAHR, Madrid, Spain, 2012), Paper-B16.
- [12] G. E. Hecker, Fundamentals of vortex intake flow, in *Swirling Flow Problems at Intakes* (Taylor & Francis, London, 2017), pp. 13–38.
- [13] J. Knauss, *Swirling Flow Problems at Intakes* (Taylor & Francis, London, 2017).
- [14] D. Tenchine, C. Fournier, and Y. Dolias, Gas entrainment issues in sodium cooled fast reactors, *Nucl. Eng. Des.* **270**, 302 (2014).
- [15] B. Moudjed, J. Excoffon, R. Riva, and L. Rossi, Experimental study of gas entrainment from surface swirl, *Nucl. Eng. Des.* **310**, 351 (2016).
- [16] H. Bhatia, U. Bieder, and D. Guenadou, Rankine-vortex model based assessment of CFD methods for simulating the effect of gas entrainment observed in the hot-pool of sodium cooled fast breeder reactors, *Prog. Nucl. Energy* **137**, 103794 (2021).
- [17] A. H. Shapiro, Bath-tub vortex, *Nature (London)* **196**, 1080 (1962).
- [18] L. M. Trefethen, R. W. Bilger, P. T. Fink, R. E. Luxton, and R. I. Tanner, The bath-tub vortex in the southern hemisphere, *Nature (London)* **207**, 1084 (1965).
- [19] L. Foucault, Démonstration physique du mouvement de rotation de la terre au moyen du pendule, *C. R. Acad. Sci.* **32**, 135 (1851).
- [20] J. Boisson, D. Cébron, F. Moisy, and P.-P. Cortet, Earth rotation prevents exact solid-body rotation of fluids in the laboratory, *Europhys. Lett.* **98**, 59002 (2012).
- [21] H. A. Einstein and H. Li, Steady vortex flow in a real fluid, in *Proceedings of the Heat Transfer and Fluid Mechanics Institute* (Stanford University Press, 1951), pp. 33–43.
- [22] W. S. Lewellen, A solution for three-dimensional vortex flows with strong circulation, *J. Fluid Mech.* **14**, 420 (1962).
- [23] H. J. Lugt, *Vortex Flow in Nature and Technology* (Wiley-Interscience, New York, 1983).
- [24] T. S. Lundgren, The vortical flow above the drain-hole in a rotating vessel, *J. Fluid Mech.* **155**, 381 (1985).
- [25] S. Shingubara, K. Hagiwara, R. Fukushima, and T. Kawakubo, Vortices around a sinkhole: Phase diagram for one-celled and two-celled vortices, *J. Phys. Soc. Jpn.* **57**, 88 (1988).
- [26] L. K. Forbes and G. C. Hocking, The bath-plug vortex, *J. Fluid Mech.* **284**, 43 (1995).
- [27] A. Andersen, T. Bohr, B. Stenum, J. J. Rasmussen, and B. Lautrup, Anatomy of a Bathtub Vortex, *Phys. Rev. Lett.* **91**, 104502 (2003).
- [28] P. A. Tyvand and K. B. Haugen, An impulsive bathtub vortex, *Phys. Fluids* **17**, 062105 (2005).
- [29] A. Andersen, T. Bohr, B. Stenum, J. Juul Rasmussen, and B. Lautrup, The bathtub vortex in a rotating container, *J. Fluid Mech.* **556**, 121 (2006).
- [30] Y. A. Stepanyants and G. H. Yeoh, Burgers–Rott vortices with surface tension, *Z. Angew. Math. Phys.* **59**, 1057 (2008).
- [31] Y. A. Stepanyants and G. H. Yeoh, Stationary bathtub vortices and a critical regime of liquid discharge, *J. Fluid Mech.* **604**, 77 (2008).
- [32] L. Bøhling, A. Andersen, and D. Fabre, Structure of a steady drain-hole vortex in a viscous fluid, *J. Fluid Mech.* **656**, 177 (2010).
- [33] S. Yukimoto, H. Niino, T. Noguchi, R. Kimura, and F. Y. Moulin, Structure of a bathtub vortex: Importance of the bottom boundary layer, *Theor. Comput. Fluid Dyn.* **24**, 323 (2010).
- [34] Y.-C. Chen, S.-L. Huang, Z.-Y. Li, C.-C. Chang, and C.-C. Chu, A bathtub vortex under the influence of a protruding cylinder in a rotating tank, *J. Fluid Mech.* **733**, 134 (2013).
- [35] M. R. Foster, Asymptotic theory for a bathtub vortex in a rotating tank, *J. Fluid Mech.* **749**, 113 (2014).
- [36] A. Duinmeijer, G. Oldenziel, and F. Clemens, Experimental study on the 3D-flow field of a free-surface vortex using stereo PIV, *J. Hydraul. Res.* **58**, 105 (2020).
- [37] H. P. Greenspan and L. N. Howard, On a time-dependent motion of a rotating fluid, *J. Fluid Mech.* **17**, 385 (1963).
- [38] E. R. Benton and A. Clark, Jr., Spin-up, *Ann. Rev. Fluid Mech.* **6**, 257 (1974).

- [39] W. Yang, I. Delbende, Y. Fraigneau, and L. Martin Witkowski, Large axisymmetric surface deformation and dewetting in the flow above a rotating disk in a cylindrical tank: Spin-up and permanent regimes, *Phys. Rev. Fluids* **5**, 044801 (2020).
- [40] A. Savitzky and M. J. E. Golay, Smoothing and differentiation of data by simplified least squares procedures, *Anal. Chem.* **36**, 1627 (1964).
- [41] R. Bergmann, A. Andersen, D. van der Meer, and T. Bohr, Bubble Pinch-Off in a Rotating Flow, *Phys. Rev. Lett.* **102**, 204501 (2009).
- [42] K. Ito, H. Ohshima, T. Sakai, and T. Kunugi, CFD-based evaluation of interfacial flows, in *Computational Fluid Dynamics* (IntechOpen, London, 2010), pp. 133–156.
- [43] E. Guyon, J.-P. Hulin, L. Petit, and C. D. Mitescu, *Physical Hydrodynamics* (Oxford University Press, New York, 2015).
- [44] Y.-L. Chen, C. Wu, M. Ye, and X.-M. Ju, Hydraulic characteristics of vertical vortex at hydraulic intakes, *J. Hydrodyn.* **19**, 143 (2007).